Supporting Information: Integrated Digital Microfluidics NMR Spectroscopy: A key step towards automated *in-vivo* metabolomics

Amy Jenne,[1,2] Sebastian von der Ecken,[1,3] Vincent Moxley-Paquette,[2] Ronald Soong,[2] Ian Swyer,[1] Monica Bastawrous,[2] Falko Busse,[4] Wolfgang Bermel,[4] Daniel Schmidig,[5] Till Kuehn,[5] Rainer Kuemmerle,[5] Danijela Al Adwan-Stojilkovic,[5] Stephan Graf,[5] Thomas Frei,[5] Martine Monette,[6] Aaron R. Wheeler,[1,7,8*] and Andre J. Simpson,[1,2*]

[1] Department of Chemistry, University of Toronto, 80. St. George Street, Toronto, Ontario, Canada, M5S 3H6
[2] Environmental NMR Center, University of Toronto Scarborough, 1265 Military Trail, Scarborough, Ontario, M1C 1A4
[3] Nicoya, B-29 King Street East, Kitchener, Ontario, Canada, N2G 2K4
[4] Bruker BioSpin GmbH, Rudolf-Plank-Str. 23, 76275 Ettlingen, Germany
[5] Bruker BioSpin AG, Industriestrasse 26, 8117 Fällanden, Switzerland
[6] Bruker Canada Ltd, 2800 High Point Drive, Milton, Ontario, L9T 6P4
[7] Donnelly Centre for Cellular and Biomolecular Research, University of Toronto, 160 College Street, Toronto, Ontario, Canada, M5S 3E1
[8] Institute for Biomedical Engineering, University of Toronto, 164 College Street, Toronto, Ontario, Canada, M5S 3G9

*Email: aaron.wheeler@utoronto.ca
*Email: andre.simpson@utoronto.ca

Table of Contents

Further Methods

Reagents
Unless otherwise specified, chemical reagents were purchased from SigmaAldrich (St. Louis, Missouri, U.S) aside from FluoroPel PFC 1101V, which was purchased from Cytonix, LLC (Beltsville, Maryland, U.S). Electronic components were purchased from Digi-Key (Thief River Falls, Minnesota, U.S).

Samples
^{13}C-D-Glucose: Standard to test microcoil performance. 500 mM sample of ^{13}C-D-Glucose (99% isotopically enriched, purchased from Silantes, GmbH) in 99% purity D_2O.
Sucrose: Standard to test microcoil performance. Solution was 1.5 M of D-Sucrose in H_2O.

Microcoil Design and Milling
Both horizontal and vertical microcoils were machined using the 3-axis mode of the MiRA6 as previously described.[1] All modeling was completed using Rhinoceros 6® and tool paths were programmed using the MadCAM® plugin. Each microcoil was machined from Cuflon® (Polyflon) with a 1/16" thick PTFE dielectric and 17.4 μm thick layers of copper (the PTFE layer is sandwiched between two copper layers). During initial testing, both vertical and horizontal microcoils had a built-in 3 mm diameter and 1.58 mm deep circular sample well. Once completed, each microcoil was dual-tuned/matched to ^{1}H and ^{13}C using a modified TXI probe body (Bruker, Switzerland). Since the Cuflon® contains copper on both sides, the copper layer opposite to the side containing the microcoil was grounded to maximize B_1 field penetration into the sample.[1,2]

The horizontal Strip design was 1 x 4 mm, where the vertical Strips were created to be 1 x 7 mm with the same sample well as the horizontal coils, fitting three organisms, and 1 x 9 mm with a 2 mm rectangular well allowing five organisms. The Spiral coil design explored in this study was a 2-turn coil with a 3 mm outer diameter (O.D.), 200 μm thick windings, and 300 μm spacing. Another design includes two square-shaped spiral coils (with opposing turns) that are right next to each other, referred to as the "Butterfly" coil here.[3] For this coil, the sample holder is situated between the two coils. Each coil of the Butterfly coil had 1.5 turns, a 2 mm O.D., 200 μm windings, and 200 μm spacing.

Simulations
Microcoil simulations were generated using Feko version 2022.0.2 (Hyperworks, Altair Michigan, U.S.). The model was designed as the coils described above. The material was selected from the Feko media library. The model was excited using an edge port of 1 V, phase 0, and a reference impedance of 50 Ohms. A second edge port with a 50 Ohm load was used as the terminating end. Method of moments (full wave solution of Maxwell's integral equations) were used, and calculations were performed at 500 MHz. The B_1 simulations were measured on a normalized scale of magnetic flux density (-30 to -40 dB).

Figure S1 shows the three horizontal coils shapes, their SNR, nutation curves, and magnetic flux density simulations of B_1 field penetration. In addition, to the radiofrequency coils, a special pulsed field gradient coil was constructed (see Figure S1a inset), this served a dual purpose: 1) it allowed larger DMF chips to the used by maximizing the horizontal space, and 2) it allowed the droplets and coil to be seen through the side of the gradient when in vertical configuration.

Results and Discussion

Horizontal Microcoils
As a reminder, five microcoils were created that can be utilized with DMF inside a modified NMR probe. Three were horizontal, and shaped as a Strip,[4] Spiral,[5] and Butterfly,[3] (see Figure S1), each with a 3 mm round sample well. For comparison, the other two were vertically oriented strip coils with differing sample wells (see text in main paper).

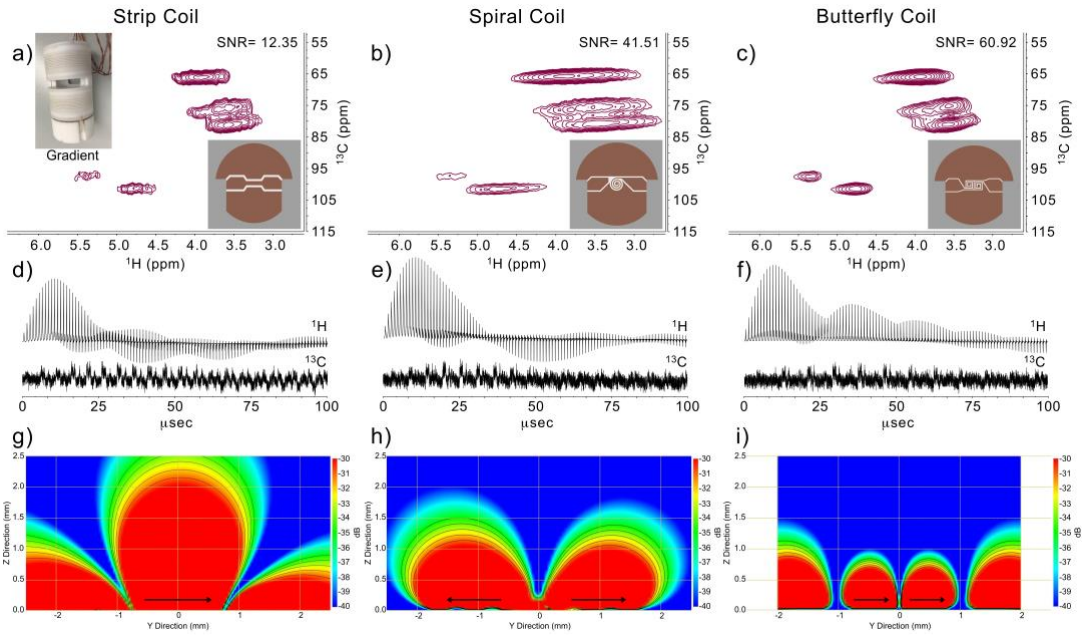

Figure S1. Comparison of three different structures horizontal microstrip coils. a-c) 2D HMQC of 500 mM ^{13}C-D-Glucose with the measured SNR and an image of the coil, a) Strip with the new pulsed field gradient seen as an inset, b) Spiral, and c) Butterfly respectively. d-f) the ^{1}H and ^{13}C nutation curves of each coil, proton was measured with D-Sucrose and carbon with ^{13}C-D-Glucose. g-h) Feko simulations of the normalized magnetic flux density from -30 to -40 dB. Each black line along the simulation represents a 10% decrease in the magnetic flux density relative to the maximum at the surface. For simplicity, only the B_1 field components important in this study (i.e., those parallel to the surface which can excite the spins) are shown. Black arrows indicate the main direction of the B_1 field.

Achieving excitation of the sample requires a uniform B_1 field that is oriented 90° to the B_o field.[6,7] In the case of the Strip coil, a significant B_1 field runs across the surface, which is effective for excitation even when the strip is horizontal. Unfortunately, this field is restricted to the width of the Strip, which must remain relatively narrow to effectively concentrate B_1 fields.[5] The 1 mm wide Strip is relatively wide compared to those commonly used.[8] Unfortunately, even with the additional lateral surface area to permit a large surface B_1 field, the performance of the Strip in the horizontal orientation was disappointing, providing an SNR that is only 12.35 for 500 mM ^{13}C-D-Glucose in HMQC. Note ^{1}H-^{13}C 2D experiments are used for coil comparison as they are central to *in-vivo* NMR of small organisms,[9] where the additional dispersion afforded by the carbon dimension is essential for detailed assignments.[10] HMQC is used here as it offers robust water suppression even when the lineshape is wide.[11]

Spiral coils also produce a strong B_1 field along the surface, and extending the windings to the center of the Spiral helps increase the B_1 field along the surface of the coil.[12] Indeed, studies of very thin substrates even when the coil plane is perpendicular to the applied magnetic field perform well.[12] Here a nearly four-fold increase in SNR over the horizontal Strip is seen. However, the line shape is quite broad (approaching ~175 Hz in proton for some peaks). This is because in the horizontal orientation the B_o field must penetrate not just the sample, but the coil and PCB substrate as well, which adds up to significant susceptibility distortions and causes the broader lineshape. In previous work thin semi-conducting films (400 µm) were studied by ^{115}In NMR using horizontal spiral coils. However, in the application the linewidths of ^{115}In were ~10 KHz,[12] and the additional broadening from the coil itself was insignificant. However, in *in-vivo* studies the full width at half height is typically ~50 Hz,[13] less than the inherent distortions caused by the coil.

Another consideration is B_1 field penetration into the sample. This is especially problematic for surface coils as spins close to the surface experience different B_1 field intensities relative to those further away.[14] For instance, with respect to inversion, if the sample is in a region that receives less than 50% of the expected B_1, spins may be flipped less than 90° and contribute a positive phase to the signal.[15] In this experiment, the sample well is 1.58 mm deep. The nutation shows relatively poor inversion consistent with previous work with surface coils where the B_1 field is not uniform across the entire sample volume,[1,14] explained by the parallel surface field running close to the surface, but not

penetrating deep into the sample. Despite the HMQC experiment employed using adiabatic inversions and being optimized for use in non-ideal B_1 fields,[16] the poor B_1 inversions seen in Figure S1d-f in both carbon and proton will undoubtedly lead to reduced HMQC performance.

Finally, a horizontal Butterfly coil was tested, which has shown promise for horizontal applications.[3] The Butterfly uses two oppositely wound coils that produce a constructive parallel B_1 field between the coils. Unlike the Spiral where the B_1 surface runs in opposite directions, the B_1 field runs in one direction (see arrows on simulations in Figure S1i). Interestingly this helps both the line shape which is reduced to as low as 146 Hz, and the SNR, which increases to 61. Unfortunately, the nutation curves still show relatively long pulse widths and poor inversion (Figure S1d-f) consistent with the partial penetration of the sample well.

Unfortunately, while the performance of the horizontal coils is promising, moving towards mass limited samples such as single organisms response of *Daphna magna* would be almost impossible in their current state. Thus, for the purposes of this study an optimized vertical coil was used in combination with DMF, which is discussed in the main paper.

Metabolite Assignments

Table S1. Metabolite Identities from Figure 3. Metabolite uses in *Daphnia magna* have been previously published.[9,10]

Number	Metabolite	Number (2)	Metabolite	Number (3)	Metabolite
1	Acetylcholine	23	Gluconic Acid	45	P-Cresol
2	Adenosine	24	Glucose-1-Phosphate	46	Phenylalanine
3	Adenosine Diphosphate (ADP)	25	Glutamic Acid	47	Phloretic Acid
4	Agmatine	26	Glutamine	48	Phosphoenolpyruvate
5	Alanine	27	Glycerol	49	Phosphothreonine
6	Aminohippuric Acid	28	Glycerol-1-Phosphate	50	Proline
7	Adenosine Monophosphate (AMP)	29	Glycine	51	Ribitol
8	Arginine	30	Histamine	52	Serine
9	Ascorbic Acid	31	Histidine	53	Spermidine
10	Asparagine	32	Isobutyric Acid	54	Succinate
11	Aspartic Acid	33	Isoleucine	55	Triacylglycerides (TAG)
12	Adenosine Triphosphate (ATP)	34	Lactic Acid	56	Threonic Acid
13	Betaine	35	Leucine	57	Threonine
14	Choline	36	L-Glutathione	58	Trigonelline
15	Citrulline	37	L-Histidinol	59	Tryptophan
16	Cysteine	38	Lysine	60	Tyramine
17	D-Galactose	39	Malic Acid	61	Tyrosine
18	D-Glucose	40	Melibiose	62	Uridine Monophosphate (UMP)
19	D-Lactose	41	Methionine	63	Uridine
20	D-Trehalose	42	Myo-inositol	64	Valine
21	D-Xylose	43	Organic Acid	65	Xanthosine
22	Gamma-aminobutyric acid (GABA)	44	Ornithine		

References

(1) Moxley-Paquette, V.; Lane, D.; Soong, R.; Ning, P.; Bastawrous, M.; Wu, B.; Pedram, M. Z.; Haque Talukder, M. A.; Ghafar-Zadeh, E.; Zverev, D.; Martin, R.; Macpherson, B.; Vargas, M.; Schmidig, D.; Graf, S.; Frei, T.; al Adwan-Stojilkovic, D.; de Castro, P.; Busse, F.; Bermel, W.; Kuehn, T.; Kuemmerle, R.; Fey, M.; Decker, F.; Stronks, H.; Sullan, R. M. A.; Utz, M.; Simpson, A. J. 5-Axis CNC Micromilling for Rapid, Cheap, and Background-Free NMR Microcoils. *Anal. Chem.* **2020**, *92* (23), 15454–15462.

(2) Chen, Y.; Mehta, H. S.; Butler, M. C.; Walter, E. D.; Reardon, P. N.; Renslow, R. S.; Mueller, K. T.; Washton, N. M. High-Resolution Microstrip NMR Detectors for Subnanoliter Samples. *Phys. Chem. Chem. Phys.* **2017**, *19* (41), 28163–28174.

(3) Lei, K. M.; Mak, P. I.; Law, M. K.; Martins, R. P. NMR–DMF: A Modular Nuclear Magnetic Resonance–Digital Microfluidics System for Biological Assays. *Analyst* **2014**, *139* (23), 6204–6213.

(4) Massin, C.; Boero, G.; Vincent, F.; Abenhaim, J.; Besse, P. A.; Popovic, R. S. High-Q Factor RF Planar Microcoils for Micro-Scale NMR Spectroscopy. *Sens. Actuators. A. Phys.* **2002**, *97–98*, 280–288.

(5) Finch, G.; Yilmaz, A.; Utz, M. An Optimised Detector for In-Situ High-Resolution NMR in Microfluidic Devices. *J. Mag. Reson.* **2016**, *262*, 73–80.

(6) van Bentum, P. J. M.; Janssen, J. W. G.; Kentgens, A. P. M. Towards Nuclear Magnetic Resonance μ-Spectroscopy and μ-Imaging. *Analyst* **2004**, *129* (9), 793–803.

(7) Haase, A.; Odoj, F.; von Kienlin, M.; Warnking, J.; Fidler, F.; Weisser, A.; Nittka, M.; Rommel, E.; Lanz, T.; Kalusche, B.; Griswold, M. NMR Probeheads for In Vivo Applications. *Concepts Magn. Reson.* **2000**, *12*, 361–388.

(8) Butler, M. C.; Mehta, H. S.; Chen, Y.; Reardon, P. N.; Renslow, R. S.; Khbeis, M.; Irish, D.; Mueller, K. T. Toward High-Resolution NMR Spectroscopy of Microscopic Liquid Samples. *Phys. Chem. Chem. Phys.* **2017**, *19* (22), 14256–14261.

(9) Bastawrous, M.; Tabatabaei-Anaraki, M.; Soong, R.; Bermel, W.; Gundy, M.; Boenisch, H.; Heumann, H.; Simpson, A. J. Inverse or Direct Detect Experiments and Probes: Which Are "Best" for in-Vivo NMR Research of 13C Enriched Organisms? *Anal. Chim. Acta.* **2020**, *1138*, 168–180.

(10) Anaraki, M. T.; Lysak, D. H.; Soong, R.; Simpson, M. J.; Spraul, M.; Bermel, W.; Heumann, H.; Gundy, M.; Boenisch, H.; Simpson, A. J. NMR Assignment of the: In Vivo Daphnia Magna Metabolome. *Analyst* **2020**, *145* (17), 5787–5800.

(11) Simpson, A. J.; McNally, D. J.; Simpson, M. J. NMR Spectroscopy in Environmental Research: From Molecular Interactions to Global Processes. *Prog. Nucl. Magn. Reson. Spectrosc.* **2011**, *58* (3–4), 97–175.

(12) Liu, W.; Lu, L.; V.F., M. Application of Surface Coil for Nuclear Magnetic Resonance Studies of Semi-Conducting Thin Films. *Rev. Sci. Instr.* **2017**, *88* (11).

(13) Fugariu, I.; Bermel, W.; Lane, D.; Soong, R.; Simpson, A. J. In-Phase Ultra High-Resolution In Vivo NMR. *Angew. Chemie Int. Ed.* **2017**, *56* (22), 6324–6328.

(14) Fugariu, I.; Soong, R.; Lane, D.; Fey, M.; Maas, W.; Vincent, F.; Beck, A.; Schmidig, D.; Treanor, B.; Simpson, A. J. Towards Single Egg Toxicity Screening Using Microcoil NMR. *Analyst* **2017**, *142* (24), 4812–4824.

(15) Bastawrous, M.; Gruschke, O.; Soong, R.; Jenne, A.; Gross, D.; Busse, F.; Nashman, B.; Lacerda, A.; Simpson, A. J. Comparing the Potential of Helmholtz and Planar NMR Microcoils for Analysis of Intact Biological Samples. *Anal. Chem.* **2022**, *94* (23), 8523–8532.

(16) Moxley-Paquette, V.; Wu, B.; Lane, D.; Bastawrous, M.; Ning, P.; Soong, R.; de Castro, P.; Kovacevic, I.; Frei, T.; Stuessi, J.; al Adwan-Stojilkovic, D.; Graf, S.; Vincent, F.; Schmidig, D.; Kuehn, T.; Kuemmerle, R.; Beck, A.; Fey, M.; Bermel, W.; Busse, F.; Gundy, M.; Boenisch, H.; Heumann, H.; Nashman, B.; Dutta Majumdar, R.; Lacerda, A.; Simpson, A. J. Evaluation of Double-Tuned Single-Sided Planar Microcoils for the Analysis of Small 13C Enriched Biological Samples Using 1H-13C 2D Heteronuclear Correlation NMR Spectroscopy. *Mag. Reson. Chem.* **2022**, *60* (3), 386–397.